

RESEARCH PAPER

Influence of CuO Nanoparticles on the Structural, Optical and Thermal Properties of CMC-PVP Films

Aws Shukur Hussien ^{*}, Adnan Raad Ahmed

Department of Physics, College of Education for Pure Science, University of Tikrit, Iraq

ARTICLE INFO

Article History:

Received 23 September 2024

Accepted 19 December 2024

Published 01 January 2025

Keywords:

CMC

CuO NPs

FTIR

Optical

PVP

Thermal Analysis

ABSTRACT

Using the precipitation process, copper oxide nanoparticles (CuO NPs) were created at different calcination temperatures of (400, 600, and 800) °C. Polymeric films (CMC-PVP) incorporating (CuO NPs) were fabricated using the casting method with weight ratios of (3, 5, 7, and 9) %. The film's thickness measured (45±1) μm. The FE-SEM measurements indicated the copper oxide phase is achieved at (400°C), and as the temperature rises, the crystallinity and particle size both increase at (600°C) and (800°C) calcination temperatures, and their propensity for agglomeration and irregular flake-like morphologies. The optical and thermal characteristics of films reinforced with CuO nanoparticles demonstrate their influence on optical transmittance over the (200-1100) nm wavelength range, alongside a decrease in energy band gap values from 4.90 eV to 4.35 eV and an increase in thermal conductivity (K) of the prepared films with escalating reinforcement ratios.

How to cite this article

Hussien A., Ahmed A. Influence of CuO Nanoparticles on the Structural, Optical and Thermal Properties of CMC-PVP Films. J Nanostruct, 2025; 15(1):239-248. DOI: 10.22052/JNS.2025.01.023

INTRODUCTION

Recent years have witnessed significant attention on the investigation and enhancement of blends of polymers to augment the characteristics of polymeric materials [1, 2]. Polymer blends consist of the mixing of two or more types of polymers to produce a novel material with tailored properties. The fusion of polymers facilitates the integration of advantageous characteristics from several polymers. [3,4]. The primary benefits of polymer blends are the customization of mechanical strength, thermal properties, dissolution stages, permeability, and processability [5]. Hybrid materials that include a combination of polymers and inorganic nanofillers are known as polymer blend nanocomposites [6].

^{*} Corresponding Author Email: awsshukur12@gmail.com

Nanoparticles of metals and oxides, clay, silica, carbon nanotubes, and graphene are among the most common inorganic nanofillers [7]. Blends of polymers with nanofillers, such as metal oxide-based nanocomposites, exhibit considerable enhancements in strength, stability, and barrier capabilities. These nanocomposites have created new opportunities for the utilization of high-quality materials in diverse applications [8,9]. The molecular bridges of nanocomposites are formed by the interaction of the nanoparticle filler with the polymer within the polymer [10]. Here come the enhanced structural, electrical, and optical capabilities of the nanocomposite [11]. CMC is a cellulose-based water-soluble polymer. Because of



This work is licensed under the Creative Commons Attribution 4.0 International License.

To view a copy of this license, visit <http://creativecommons.org/licenses/by/4.0/>.

its high viscosity, it finds usage in many industrial parts, including paper, pharmaceuticals, food, agriculture, barriers, and more. A thick solution can be prepared by dissolving hygroscopic CMC in either hot or cold water. If you're looking for a water-soluble glue, softener, or resin, the CMC is a fantastic choice [12,13]. A synthetic polymer derived from the monomer polyvinylpyrrolidone, PVP is also called povidone. It is soluble in water. This PVP material Its glass transition temperature (T_g) is high, and its structure is semi-crystalline [14]. The unusual features of PVP, which include its ability to form stable complexes with numerous molecules, have led to its diverse applications. Its proximity in the pyrrolidone group is another contributing factor. In addition to its usage as a film-forming component, PVP is utilized as an adhesive ingredient in personal care products and as a viscosity enhancer [15,16]. The incorporation of nanoparticles into synthetic and polymer films has proven to be an effective approach for improving their properties [17]. Copper oxides are recognized for their diverse applications, they are p-type semiconductors characterized by a small energy gap, ease of production, non-toxic properties, and excellent electrical and optical performance [18,19]. CuO nanoparticles are receiving significant attention owing to their prospective uses across various domains, including electrical and optical devices, such as field-effect transistors, electrochemical cells, gas sensors, and nanodevices for catalytic reactions, to develop these materials for application as gas detection materials, solar cells, and photonic switches, CuO nanoparticles are mixed with different polymers [19, 20]. In this study, the polymeric mixture was made with PVP and CMC in an equal proportion, and CuO nanoparticles were added to it at concentrations of (3, 5, 7, and 9) %. This study's goal is to synthesize of (CuO NPs) via the precipitation method and is to examine how the physical, optical, and thermal characteristics of the polymer blend are affected by the addition of copper nanoparticles.

MATERIALS AND METHODS

Used Material

Copper (II) chloride dihydrate. ($\text{CuCl}_2 \cdot 2\text{H}_2\text{O}$) in addition to a (25%) ammonia hydroxide (NH_4OH) solution. It was acquired from Sigma Aldrich without additional putrefaction processes., CMC The product is made by SINOCMC and a Chinese

firm with type (CAS.NO.9004-32-4), PVP, as well as by DIERVO and a UK firm, with (4000) its molecular weight.

The Preparation of (CuO NPs)

The (CuO NPs) were prepared via the precipitation method by adhering to the following procedures: (0.5M) of the copper (II) chloride dihydrate ($\text{CuCl}_2 \cdot 2\text{H}_2\text{O}$) was dissolved in (100 ml) of distilled water while continually stirring with a magnetic stirrer at (50°C), allowing the solution to equilibrate for thirty minutes to achieve homogeneity. A solution of ammonium hydroxide (NH_4OH) was incrementally administered dropwise utilizing a (100 ml) graduated burette. The diluted ammonium hydroxide was positioned in the burette, and distillation was conducted at a rate of (2 ml) per minute with constant agitation. Upon completion of the distillation process, the resultant solution will exhibit a pH concentration of (10) while being subjected to continuous heating at (50°C) to facilitate water evaporation. The solution is subsequently filtered via filter paper and rinsed multiple times with distilled water. The resultant material has been dried for four hours at (200°C), then underwent calcination at (400, 600, and 800) $^\circ\text{C}$ for four hours to yield copper oxide nanoparticles (CuO NPs).

The Preparation of Nanocomposites Containing (CMC-PVP: CuO)

Each component, CMC and PVP, weighed (0.5 g) and was dissolved in (50 ml) of distilled water at (70°C) and (40°C), respectively. Once each ingredient had dissolved, it was mixed with the others and left to agitate for another two hours. Then, the solutions were agitated for another hour after adding (CuO NPs) at concentrations of (3, 5, 7, and 9) wt%. Once the mixture was mixed, it was put into 90-millimeter diameter flat plastic Petri dishes and allowed to dry at room temperature for two days. The prepared homogeneous films were removed using tweezers. As the samples were free of bubbles and without thermal damage. In order to characterize CMC-PVP and CMC-PVA:CuO materials, the films' thickness was measured with a micrometer, revealing an average thickness of (45 ± 1) μm . The Shimadzu FTIR-8400S Fourier Transform Infrared Spectrophotometer was used. A dual-beam UV/visible spectrophotometer made by Shimadzu Japan, model UV-160 A, was used to measure absorption and transmission.

RESULT AND DISCUSSION

Structural Analysis

FE-SEM Analysis

The surface morphological characteristics, in

addition to the shape and particle size distribution of the prepared samples represented by the nanocrystalline powder (CuO NPs) synthesized by chemical precipitation, were evaluated. This test

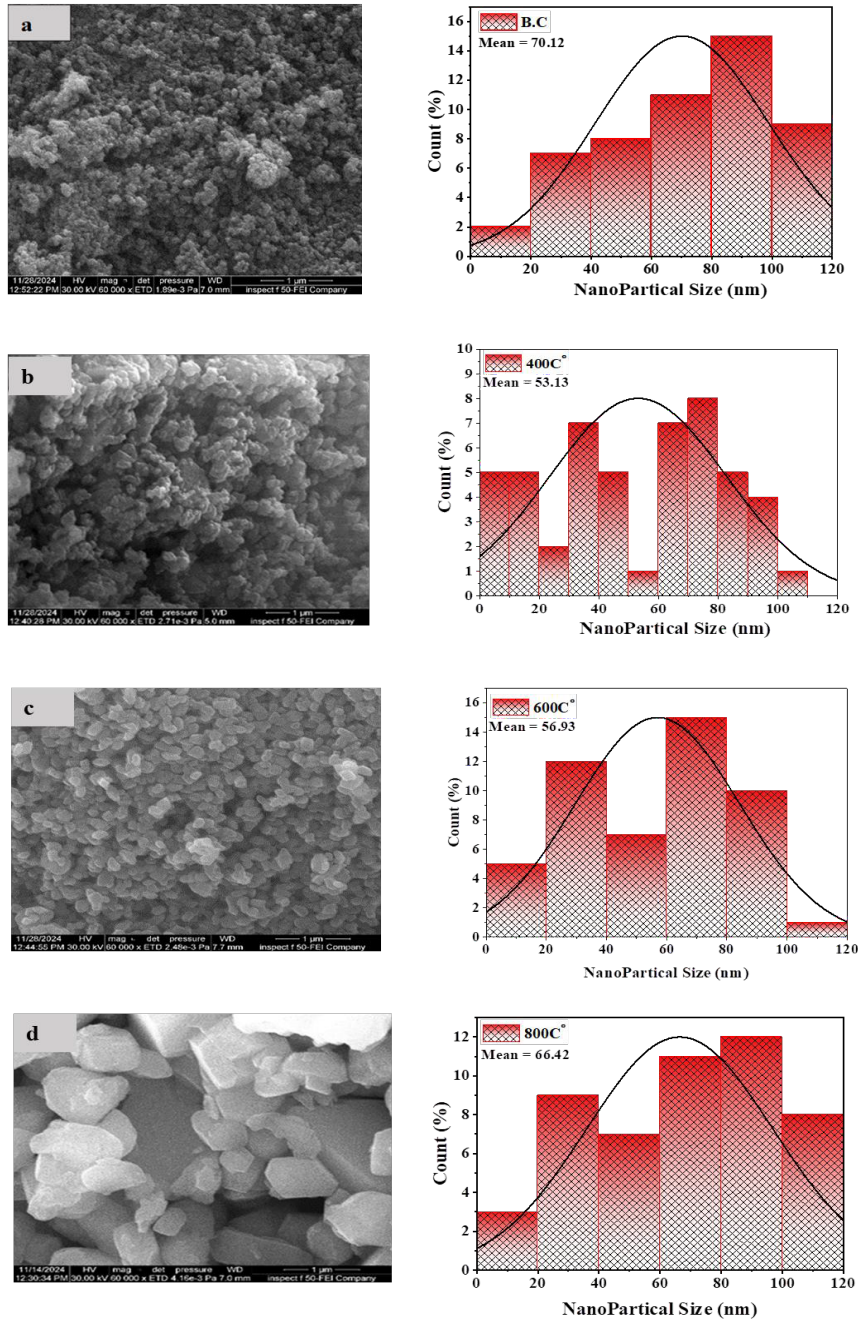


Fig. 1. Microscopic images and distribution of the (CuO NPs) powder (a Before Calcination (b at (400°C) (c at (600°C) (d at (800°C).

was conducted on the powder before and after calcination. at different temperatures (400, 600, 800) °C using an (FE-SEM) device. Fig. 1 illustrates the microscopic pictures and the distribution of copper oxide nanoparticles (CuO NPs) prior to and subsequent to the calcination process at varying temperatures of (400, 600, and 800) °C. The

microscopic images of the powder, generated prior to heat treatment and dried at (200°C), exhibit dense nanoparticle aggregates with an uneven morphology and irregularly shaped nanoparticles. The explanation for this lies in the unpredictable characteristics of the chlorinated compounds in the formula $(Cu_2(OH)_3Cl)$ and the failure of the

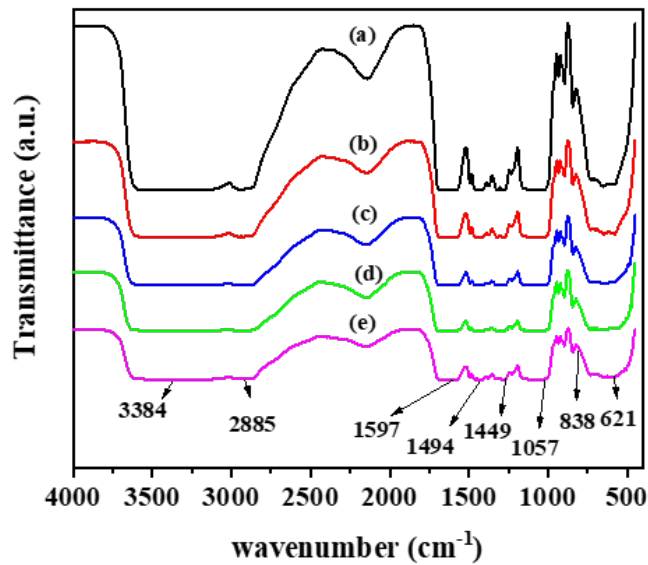


Fig. 2. FTIR spectrum of the prepared (CMC-PVP) films, both pure and reinforced with different weight percentages (wt%) of calcined particles, where (a) Pure, (b) 3%, (c) 5%, (d) 7%, (e) 9%.

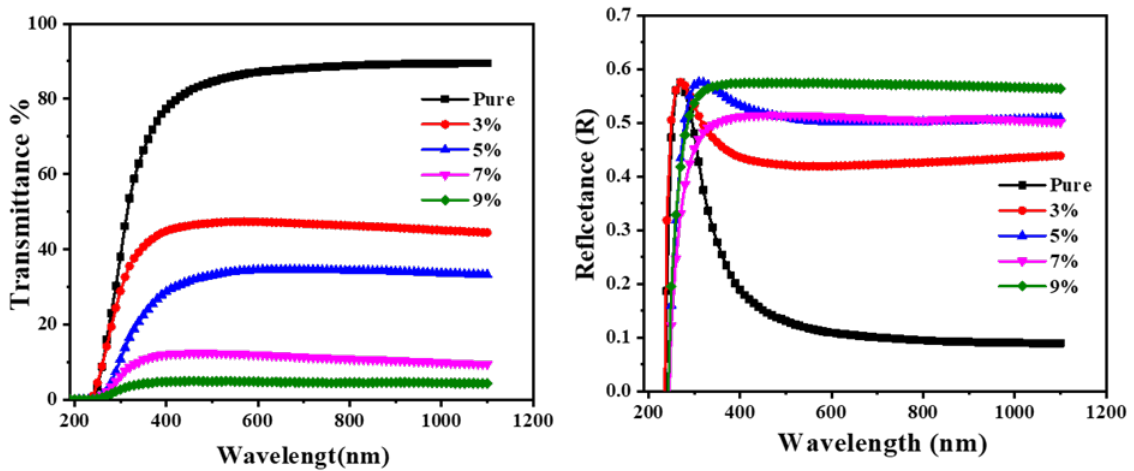


Fig. 3. Values of (T %) & (R) for the pure and reinforced (CMC-PVP) mixture.

hydroxide to decompose into its final state during the powder's drying at (200°C), notwithstanding the emergence of certain nanoparticles due to the drying process. [21, 22]. Following the initial heat treatment at (400°C), an enhancement in the crystallization process is observed, resulting in the development of a crystalline phase and dense spherical copper oxide nanoparticles that combine into spherical forms, with an increase in the thermal treatment temperature to (600°C). We find that the crystalline phase of the nanoparticles has become complete, and it was observed that the particles are spherical, well-dispersed, and almost uniformly consistent with the specified and unified crystalline structure. Regarding (800°C), we notice an increase in the size of the nanoparticles, leading to the formation of irregular shapes resembling flakes. Nonetheless, several small particles adhered to the larger spherical particles, and the degree of crystallization increased. There is also a higher tendency for agglomerates to be surrounded by small nanoparticles. This is attributed to the fact that the phase transformation of the agglomerates heavily depends on the calcination temperature, concentration, and interfacial friction during sintering [23–25].

FT-IR Analysis

Fig. 2 shows the (IR) spectrum of the pure blends (CMC-PVP) films and those reinforced with weight percentages (3, 5, 7, 9) wt% calcined at (800°C) of (CuO NPs) in the wavenumber range (400-4000) cm^{-1} . The infrared (IR) spectrum displays the

main packages and effective functional groups associated with the (CMC) and (PVP) polymers. The infrared spectrum of the (CMC) polymer contains a hydroxyl group with a stretching (-OH) at the wavenumber (3384) cm^{-1} . A hydrocarbon group stretching (C-H) for the (-CH₂) groups at the wavenumber (2885) cm^{-1} . In addition to a carbonyl group stretching (C=O) at the wavenumber (1597) cm^{-1} [26]. The main spectra of the polymer (PVP) are attributed to two vibrational bands, the first at (1273) cm^{-1} and the second at the wavenumber (1433) cm^{-1} , resulting from the asymmetric stretching and bending of (-CH₂). Observation of two vibration patterns resulting from the stretching of (C-O) and (C-C) at the wavenumbers (1057) cm^{-1} and (838) cm^{-1} , respectively [27–29]. A small band is also observed at the stretching (1449) cm^{-1} attributed to (C=N) in the pyridine structure within (PVP). Regarding the absorption band at the stretching (621) cm^{-1} attributed to (Cu-O). It indicates that the reinforcement with copper oxide particles has increased the intensity of the hydrocarbon group (-CH) range. This indicates the interaction of CuO nanoparticles with the active groups of the polymer blend. [30].

Optical analysis

The study of transmittance and reflectance Spectra helps in understanding and improving the polymer's composition and energy gap. Fig. 3 shows the transmittance. and reflectance spectra of the pure blend (CMC-PVP) and the blend reinforced with varying weight ratios of calcined copper oxide nanoparticles (CuO NPs) at

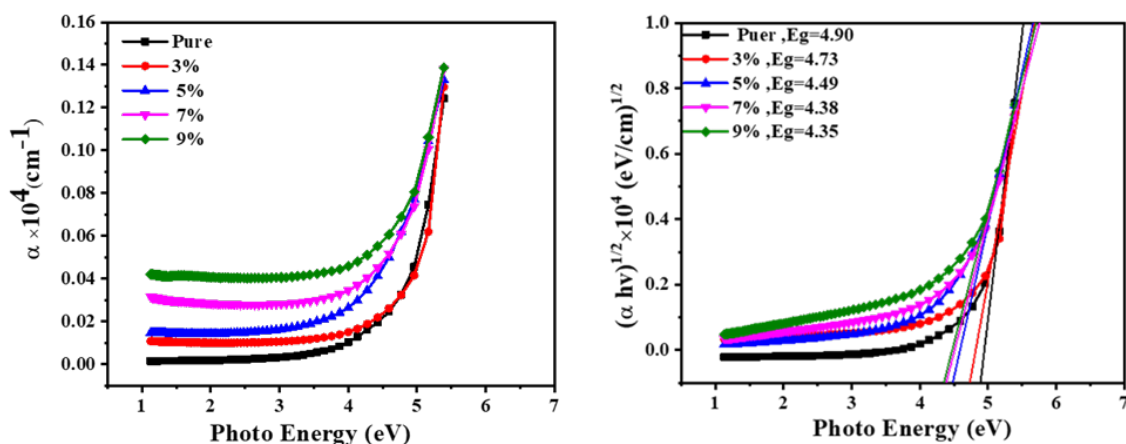


Fig. 4. Values of (α) & (E_g) for the pure and reinforced (CMC-PVP) mixture.



a temperature of (800°C). The use of (CuO NPs) led to a decrease in the permeability of the (CMC-PVP) blend, with the reduction in permeability becoming more pronounced as the proportion of (CuO NPs) particles increased. The permeability of the prepared samples increases with the wavelength until it stabilizes at wavelengths higher than (650-800) nm. This is because the increase in the weight ratios of the nanoparticles leads to a higher density of the nanoparticles, which in turn increases scattering and decreases permeability, in accordance with reference [31]. On the other hand, the reflectivity of the (CMC-PVP) mixture increased with the addition of (CuO NPs). Additionally, the reflectivity decreased significantly with increasing wavelength and stabilized at a wavelength higher than (650-800) nm. This can be attributed to the absorption and scattering of the incident light by (CuO NPs) within the (CMC-PVP) mixture, where part of the incident light is absorbed and the rest is scattered [32].

The absorption coefficient (α) for the (CMC-PVP) films was calculated using Eq. 1 as shown in Fig. 4. It is clear that the absorption coefficient of the prepared samples is higher at higher photon energies and decreases with lower photon energy. The absorption coefficient increases with the increase in the proportion of (CuO NPs), this can be attributed to the increase in the number of charges carriers, leading to a higher absorption coefficient for the composite nanofilms. Additionally, the (α) is an indication of the type of electronic transition in the prepared films, as the (α) values for the (CMC-PVP: CuO) [33,34].

$$\alpha = 2.303 \frac{A}{t} \quad (1)$$

As also shown in Fig. 4, the energy gap value (E_g) for the indirect electronic transition of (CMC-PVP) films was measured according to the pure Eq. 2 at 4.90 eV. while the (E_g) values of the reinforced films decrease with increasing content of copper oxide nanoparticles. Calcined at a temperature of 800°C, the values become 4.73 eV, 4.49 eV, 4.38 eV, and 4.35 eV for reinforcement ratios of (3, 5, 7, and 9) %, respectively. With the increase in the concentration of (CuO NPs), the defects in the films become more pronounced, leading to a decrease in the energy bandgap value. A decrease in the energy gap values occurs due to these defects, which generate specific regions of energy levels within them, the optical characteristics of the produced components may alter as a result of surface imperfections and contaminants on nanoparticles introducing extra electronic states [35].

$$\alpha h\nu = P(h\nu - E_g)^r \quad (2)$$

The values of the refractive index and extinction coefficient (n_o, k_o) for the (CMC-PVP) films were estimated using Eqs. 3 and 4. It was observed from Fig. 5 that as the concentration of (CuO NPs) increased, both the (n_o, k_o) increased. The (n_o) showed an upward trend, with the increase in incoming photon energy leading to an increase in the (n_o) of the prepared films. Additionally, the rise in refractive index values with increased

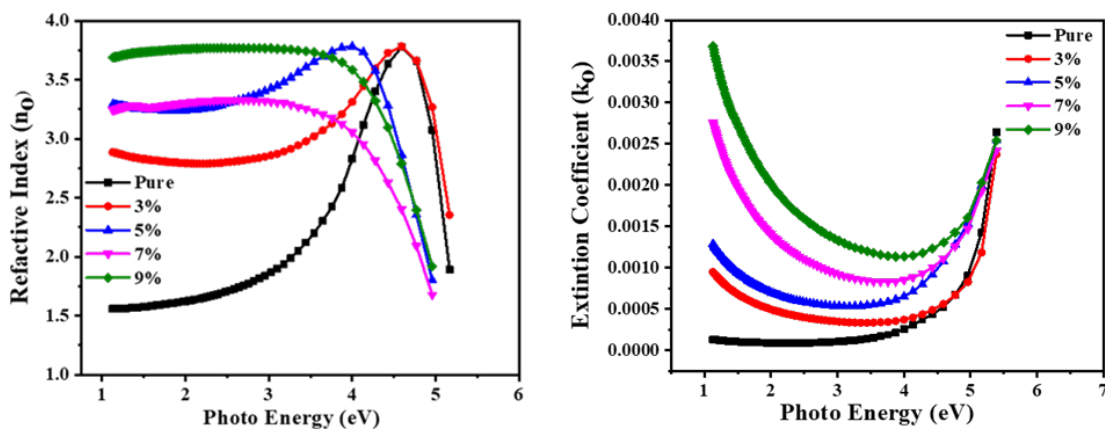


Fig. 5. Values of (n_o) & (k_o) for the pure and reinforced (CMC-PVP) mixture.

reinforcement is due to the increase in nanoparticle density, also known as packing density. The increase in the loss tangent can explain the rise in the absorption coefficient (α), as there is a strong relationship between the two variables, as agreed upon by many researchers [31, 35].

$$n_o = \left[\left(\frac{1+R}{1-R} \right)^2 - (k_o^2 + 1) \right]^{1/2} + \frac{1+R}{1-R} \quad (3)$$

$$k_o = \alpha\lambda/4\pi \quad (4)$$

Fig. 6 illustrates the variations in the real (E_r) and imaginary (E_i) components of the dielectric constant in relation to the weight ratio of (CuO NPs) inside both pure and enhanced (CMC-PVP) composites as a function of photon energy. The findings indicate that including calcined (CuO NPs)

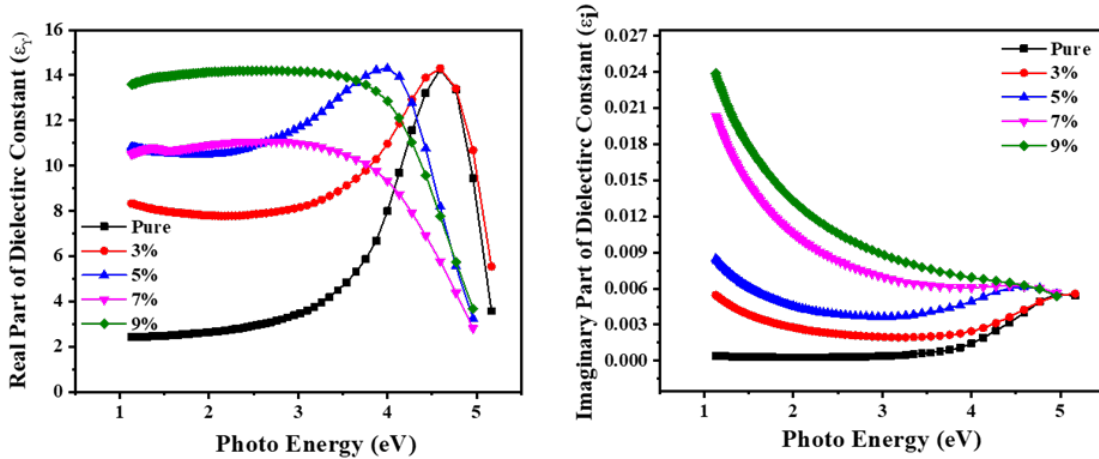


Fig. 6. Values of (E_r) & (E_i) for the pure and reinforced (CMC-PVP) mixture.

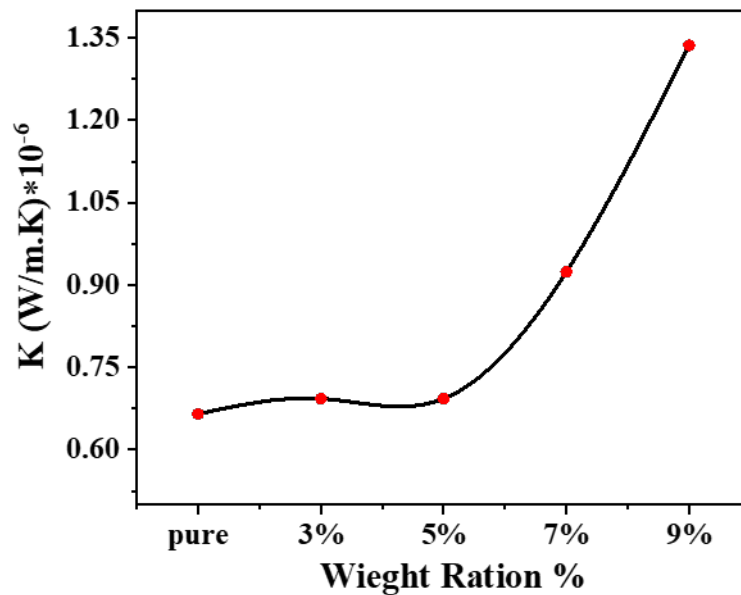


Fig. 7. Thermal conductivity values (K) for the prepared (CMC-PVP) pure and reinforced films.

Table 1. Visual measurement parameters of both pure and doped (CMC-PVP) films.

Sample	Energy Gap (eV)	($\alpha \times 10^4 \text{cm}^{-1}$) Maximum	(n_o) Maximum	(k_o) Maximum
CMC-PVP	4.90	0.12429	3.32649	0.00237
CMC-PVP: CuO NPs (3%)	4.73	0.12964	3.76775	0.00254
CMC-PVP: CuO NPs (5%)	4.49	0.13288	3.77637	0.00264
CMC-PVP: CuO NPs (7%)	4.38	0.13807	3.7809	0.00276
CMC-PVP CuO NPs (9%)	4.35	0.13887	3.78187	0.00368

Table 2. Thermal conductivity (K) values for the prepared models.

SAMPLE	K(W/M ² .K)
CMC-PVP Pure	6.64922E-7
CMC-PVP: CuO NPs (3%)	6.92934E-7
CMC-PVP: CuO NPs (5%)	6.92934E-7
CMC-PVP: CuO NPs (7%)	9.23671E-7
CMC- PVP: CuO NPs (9%)	1.33665E-6

at a temperature of (800°C) enhances the (E_r) and (E_i) components of the dielectric constant. This augmentation is ascribed to the elevated concentration of nanoparticles, which improves the absorption and scattering of incident light. Moreover, the elevated concentrations signify an enhancement in polarizability, indicating a proportionate rise in charges inside the composites. The fluctuation of these components as a function of photon energy arises from the dependence of the real component (E_r) on the absorption coefficient, whereas the imaginary component (E_i) of the dielectric constant is associated with the extinction coefficient [36, 37]. The results are displayed in Table 1.

Thermal Analysis

The evaluation of polymeric materials and their composites for thermal applications involves the analysis of their thermal conductivity as a key physical property. The thermal conductivity coefficients (K) of the synthesized films were determined utilizing the Lee's disc method [38]. Fig. 7 illustrates the thermal conductivity values (K) of the synthesized pure films (CMC-PVP) and those augmented with varying weight percentages (3, 5, 7, 9) % of (CuO NPs) calcined at (800°C).

The results indicated a progressive enhancement in the thermal conductivity coefficient (K) with the addition of (CuO NPs) to the polymer blend (CMC-PVP). The thermal conductivity coefficient (K) of the pure (CMC-PVP) film was determined

to be (6.64922×10^{-7} W/m². K) with a notable rise observed. While the greatest thermal conductivity value was recorded for the (CMC-PVP-9%CuO) film measuring (1.33665×10^{-6} W/m². K). Table 2 presents the thermal conductivity (K) values of the synthesized samples. The use of nanoparticles in polymeric materials enhances thermal conductivity values (K). The enhancement arises from the integration of nanoparticles into the polymer matrix, which occupy the structural spaces within the polymer. Furthermore, the included copper oxide nanoparticles demonstrate superior thermal conductivity relative to the unadulterated polymer mix (CMC-PVP) owing to variations in their structural makeup [39,40].

CONCLUSION

The structural properties (FE-SEM) of the employed reinforcing material (CuO NPs) illustrate the crystallization process of copper oxide particles, the completion of the crystalline phase with increasing nanoparticle size, and their propensity for agglomeration and irregular flake-like morphologies. The solution casting method has demonstrated efficacy in producing samples of pure and reinforced polymeric films, as evidenced by structural characterization that confirmed the purity of the samples and the absence of unknown bonds, alongside the characteristic interaction between the reinforcing material and the functional groups of the polymeric blend, as indicated by the FTIR results. The optical analysis

of the samples indicated that an increased addition of reinforcement correlates with elevated values of (R), (α), (n_o), and both the (E_r), (E_i) components of the dielectric constant, accompanied by a reduction in permeability values and energy gap. Thermal analysis indicates that the (K) increases with the increase in reinforcement ratios of polymeric films.

CONFLICT OF INTEREST

The authors declare that there is no conflict of interests regarding the publication of this manuscript.

REFERENCES

1. The Properties, Preparation and Applications for Carboxymethyl Cellulose (CMC) Polymer: A Review. *Diyala Journal for Pure Science*. 2022;18:167-181.
2. El Sayed AM, El-Gamal S. Synthesis and investigation of the electrical and dielectric properties of Co3O4/(CMC+PVA) nanocomposite films. *Journal of Polymer Research*. 2015;22(5).
3. Ahmed L, Zhang B, Hatanaka LC, Mannan MS. Application of polymer nanocomposites in the flame retardancy study. *J Loss Prev Process Ind*. 2018;55:381-391.
4. Alghunaim NS. Effect of CuO nanofiller on the spectroscopic properties, dielectric permittivity and dielectric modulus of CMC/PVP nanocomposites. *Journal of Materials Research and Technology*. 2019;8(4):3596-3602.
5. Xin Q, Pan Y, Zhang C, Zhang L, Dong C, Lin L, et al. An exploration of novel natural gas leak detection based on the efficient CH₄/N₂ separation of polymer blend membrane. *Sep Purif Technol*. 2024;336:126302.
6. Mohammed AA, Ahmed AR, Al-Timimi MH. Structural, Optical and Thermal Properties of (PEG/PAA:MnO₂) Nano Composites. *Technium BioChemMed*. 2022;3(2):107-119.
7. Abdelghany AM, Elamin NY, Younis S, Ayaad DM. Polyvinyl pyrrolidone/ carboxymethyl cellulose (PVP/CMC) polymer composites containing CuO nanoparticles synthesized via laser ablation in liquids. *J Mol Liq*. 2024;403:124857.
8. Jawad YM, Al-Kadhemy MFH, Salman JAS. Synthesis Structural and Optical Properties of CMC/MgO Nanocomposites. *Mater Sci Forum*. 2021;1039:104-114.
9. Damoom MM, Saeed A, Alshammari EM, Alhawsawi AM, Yassin AY, Abdulwahed JAM, et al. The role of TiO₂ nanoparticles in enhancing the structural, optical, and electrical properties of PVA/PVP/CMC ternary polymer blend: nanocomposites for capacitive energy storage. *J Sol-Gel Sci Technol*. 2023;108(3):742-755.
10. Huang C, Qian X, Yang R. Thermal conductivity of polymers and polymer nanocomposites. *Materials Science and Engineering: R: Reports*. 2018;132:1-22.
11. Wahid F, Wang H-S, Lu Y-S, Zhong C, Chu L-Q. Preparation, characterization and antibacterial applications of carboxymethyl chitosan/CuO nanocomposite hydrogels. *Int J Biol Macromol*. 2017;101:690-695.
12. Lakshmi DS, Trivedi N, Reddy CRK. Synthesis and characterization of seaweed cellulose derived carboxymethyl cellulose. *Carbohydr Polym*. 2017;157:1604-1610.
13. Benslimane A, Bahlouli IM, Bekkour K, Hammiche D. Thermal gelation properties of carboxymethyl cellulose and bentonite-carboxymethyl cellulose dispersions: Rheological considerations. *Applied Clay Science*. 2016;132-133:702-710.
14. Wang J, Liu W, Song X, Ma Y, Huang Y. Effects of added polyvinyl pyrrolidone on morphology and microstructure of multiple-phase mullite nanofibers. *Ceram Int*. 2018;44(13):15418-15427.
15. Teodorescu M, Bercea M. Poly(vinylpyrrolidone) – A Versatile Polymer for Biomedical and Beyond Medical Applications. *Polymer-Plastics Technology and Engineering*. 2015;54(9):923-943.
16. Franco P, De Marco I. The Use of Poly(N-vinyl pyrrolidone) in the Delivery of Drugs: A Review. *Polymers*. 2020;12(5):1114.
17. Hashem M, Saion E, Al-Hada NM, Kamari HM, Shaari AH, Talib ZA, et al. Fabrication and characterization of semiconductor nickel oxide (NiO) nanoparticles manufactured using a facile thermal treatment. *Results in Physics*. 2016;6:1024-1030.
18. Tamgadge YS, Talwatkar SS, Sunatkari AL, Paturkar VG, Muley GG. Studies on nonlocal optical nonlinearity of Sr–CuO–polyvinyl alcohol nanocomposite thin films. *Thin Solid Films*. 2015;595:48-55.
19. Chang M-H, Liu H-S, Tai CY. Preparation of copper oxide nanoparticles and its application in nanofluid. *Powder Technol*. 2011;207(1-3):378-386.
20. Khaorapapong N, Khumchoo N, Ogawa M. Preparation of copper oxide in smectites. *Applied Clay Science*. 2015;104:238-244.
21. Charlena C, Sugiarti S, Ardiansyah D. Synthesis and Characterization of Copper(II) Oxide (CuO-NP) Nanoparticles using Chemical Precipitation Method. *JURNAL KIMIA MULAWARMAN*. 2024;21(2):84.
22. Maensiri S, Nuansing W. Thermoelectric oxide NaCo₂O₄ nanofibers fabricated by electrospinning. *Materials Chemistry and Physics*. 2006;99(1):104-108.
23. Ali K, Sajid M, Abu Bakar S, Younis A, Ali H, Zahid Rashid M. Synthesis of copper oxide (CuO) via coprecipitation method: Tailoring structural and optical properties of CuO nanoparticles for optoelectronic device applications. *Hybrid Advances*. 2024;6:100250.
24. Chauhan A, Verma R, Batoo KM, Kumari S, Kalia R, Kumar R, et al. Structural and optical properties of copper oxide nanoparticles: A study of variation in structure and antibiotic activity. *J Mater Res*. 2021;36(7):1496-1509.
25. Kannan K, Radhika D, Nikolova MP, Sadasivuni KK, Mahdizadeh H, Verma U. Structural studies of bio-mediated NiO nanoparticles for photocatalytic and antibacterial activities. *Inorg Chem Commun*. 2020;113:107755.
26. Rajeh A, Morsi MA, Elashmawi IS. Enhancement of spectroscopic, thermal, electrical and morphological properties of polyethylene oxide/carboxymethyl cellulose blends: Combined FT-IR/DFT. *Vacuum*. 2019;159:430-440.
27. Elashmawi IS, Abdel Baieth HE. Spectroscopic studies of hydroxyapatite in PVP/PVA polymeric matrix as biomaterial. *Current Applied Physics*. 2012;12(1):141-146.
28. Teodorescu M, Bercea M, Morariu S. Biomaterials of PVA and PVP in medical and pharmaceutical applications: Perspectives and challenges. *Biotechnol Adv*. 2019;37(1):109-131.
29. Chen W, Chen J, Feng Y-B, Hong L, Chen Q-Y, Wu L-F, et al. Peroxidase-like activity of water-soluble cupric

- oxide nanoparticles and its analytical application for detection of hydrogen peroxide and glucose. *The Analyst*. 2012;137(7):1706.
30. Ramani RV, Ramani BM, Sapia AD, Dhruv D, Markna JH. Synthesis and Optical Characterization of CuO Nanoparticles on Solar Borosilicate Glass. *Journal of Nano Research*. 2015;37:68-73.
 31. Mawat AJ, Al-Timimi MH, Albanda WH, Abdullah MZ. Morphological and optical properties of Mg_{1-x}Cd_x nanostructured thin films. *AIP Conference Proceedings: AIP Publishing*; 2023. p. 090019.
 32. Alias SS, Ismail AB, Mohamad AA. Effect of pH on ZnO nanoparticle properties synthesized by sol-gel centrifugation. *J Alloys Compd*. 2010;499(2):231-237.
 33. Agool IR, Kadhim KJ, Hashim A. Fabrication of new nanocomposites: (PVA-PEG-PVP) blend-zirconium oxide nanoparticles) for humidity sensors. *International Journal of Plastics Technology*. 2017;21(2):397-403.
 34. Hashim A, Hadi Q. Structural, electrical and optical properties of (biopolymer blend/titanium carbide) nanocomposites for low cost humidity sensors. *Journal of Materials Science: Materials in Electronics*. 2018;29(13):11598-11604.
 35. Sarode KM, Bachhav SG, Patil UD, Patil DR. Synthesis and Characterization of MoS₂-Graphene Nanocomposite. *Techno-Societal 2016: Springer International Publishing*; 2017. p. 629-634.
 36. Morsi MA, Pashameah RA, Sharma K, Alzahrani E, Farea MO, Al-Muntaser AA. Hybrid MWCNTs/Ag Nanofiller Reinforced PVP/CMC Blend-Based Polymer Nanocomposites for Multifunctional Optoelectronic and Nanodielectric Applications. *Journal of Polymers and the Environment*. 2022;31(2):664-676.
 37. Ayoub RH, Timimi MHA-, Esmaeil Jalali L. Characterization of Morphological and Optical Properties of MgO:SnO₂ Nanostructure Thin Films. *Academic Science Journal*. 2024;2(4):307-319.
 38. Chen C, Jiang Y, Guo J, Wu X, Zhang W, Wu S, et al. Solvent-Assisted Low-Temperature Crystallization of SnO₂ Electron-Transfer Layer for High-Efficiency Planar Perovskite Solar Cells. *Adv Funct Mater*. 2019;29(30).
 39. Gaber A, Abdel-Rahim MA, Abdel-Latif AY, Abdel-Salam MN. Influence of Calcination Temperature on the Structure and Porosity of Nanocrystalline SnO₂ Synthesized by a Conventional Precipitation method. *International Journal of Electrochemical Science*. 2014;9(1):81-95.
 40. Jones DRH, Ashby MF. *Engineering Materials and Their Properties*. Engineering Materials 1: Elsevier; 2019. p. 1-12.